Sialylation of Asparagine 612 Inhibits Aconitase Activity during Mouse Sperm Capacitation; a Possible Mechanism for the Switch from Oxidative Phosphorylation to Glycolysis

Authors

Ana Izabel Silva Balbin Villaverde, Rachel A. Ogle, Peter Lewis, Vincenzo Carbone, Tony Velkov, Jacob K. Netherton, and Mark A. Baker

Correspondence

Mark.Baker@newcastle.edu.au

In Brief

Following ejaculation, sperm undergo a series of post-translational modifications that enable the cell to find and fertilize and egg; a process known as capacitation. Here we show that the mitochondrial enzyme Aconitase becomes sialylated during capacitation. Consequently, this inhibits Aconitase activity. This may be a mechanism by which sperm switch from an oxidative to glycolytic dependent cell.

Graphical Abstract

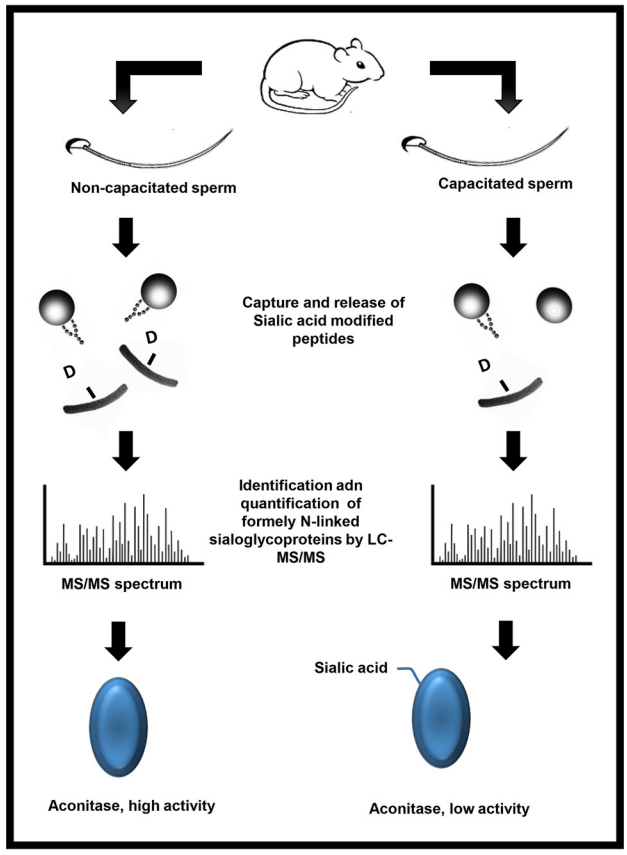

Highlights

- During sperm capacitation, 6 proteins become de-silyated, whilst one becomes silyated.
- Loss of sialylated from Endothelial lipase results in reduction of activity.
- Silyation of N612 on Aconitase causes loss of activity.
- Silyation of Aconitase may explain the switch from oxidative phosphorylation to glycolysis during capacitation.

Silva Balbin Villaverde et al., 2020, Mol Cell Proteomics *19(11),* 1860–1875
November 2020
https://doi.org/10.1074/mcp.RA120.002109

Sialylation of Asparagine 612 Inhibits Aconitase Activity during Mouse Sperm Capacitation; a Possible Mechanism for the Switch from Oxidative Phosphorylation to Glycolysis

Ana Izabel Silva Balbin Villaverde[1], Rachel A. Ogle[1], Peter Lewis[2], Vincenzo Carbone[3], Tony Velkov[4], Jacob K. Netherton[1], and Mark A. Baker[1,*]

After ejaculation, mammalian spermatozoa must undergo a process known as capacitation in order to successfully fertilize the oocyte. Several post-translational modifications occur during capacitation, including sialylation, which despite being limited to a few proteins, seems to be essential for proper sperm-oocyte interaction. Regardless of its importance, to date, no single study has ever identified nor quantified which glycoproteins bearing terminal sialic acid (Sia) are altered during capacitation. Here we characterize sialylation during mouse sperm capacitation. Using tandem MS coupled with liquid chromatography (LC–MS/MS), we found 142 nonreductant peptides, with 9 of them showing potential modifications on their sialylated oligosaccharides during capacitation. As such, *N*-linked sialoglycopeptides from C4b-binding protein, endothelial lipase (EL), serine proteases 39 and 52, testis-expressed protein 101 and zonadhesin were reduced following capacitation. In contrast, mitochondrial aconitate hydratase (aconitase; ACO2), a TCA cycle enzyme, was the only protein to show an increase in Sia content during capacitation. Interestingly, although the loss of Sia within EL (N62) was accompanied by a reduction in its phospholipase A_1 activity, a decrease in the activity of ACO2 (*i.e.* stereospecific isomerization of citrate to isocitrate) occurred when sialylation increased (N612). The latter was confirmed by N612D recombinant protein tagged with both His and GFP. The replacement of Sia for the negatively charged Aspartic acid in the N612D mutant caused complete loss of aconitase activity compared with the WT. Computer modeling show that N612 sits atop the catalytic site of ACO2. The introduction of Sia causes a large conformational change in the alpha helix, essentially, distorting the active site, leading to complete loss of function. These findings suggest that the switch from oxidative phosphorylation, over to glycolysis that occurs during capacitation may come about through sialylation of ACO2.

Sperm capacitation is a phenomenon first described by Chang (1), and Austin (2) who demonstrated that freshly ejaculated spermatozoa are unable to fertilize the oocyte immediately. Rather, a period within the female reproductive tract was required (1). During this period, it is evident that spermatozoa undergo a series of biochemical and metabolic changes to become fully capable of fertilizing the egg (3–5). From a metabolic perspective, Fraser and Lane first described the phenomenon of a metabolic switch that occurs during capacitation (6). In this context, freshly ejaculated spermatozoa have high rates of oxygen consumption, however, during *in vitro* capacitation, mouse spermatozoa decrease their reliance on oxidative phosphorylation and switch over to a glycolytic pathway (6). Using different metabolic substrates, this "switch" was shown to be necessary to achieve fertilization (6). In addition, the reliance on glycolysis explain why sperm-specific glycolytic knockout mice, including GADPH (7), are infertile because of poor motility. From a biochemical perspective, it is unknown how sperm make this switch. However, considering that spermatozoa are transcriptionally and translationally silent, except for mitochondrial proteins (8), we reasoned that post-translational modifications of existing proteins would likely play a role (9).

Although the role of phosphorylation in sperm capacitation is well studied (10–12), few studies have looked at the specific role of protein glycosylation. The latter is characterized by the addition of oligosaccharide side chains via a covalent linkage either at the asparagine (Asn) residue (*N*-linked) or at the serine/threonine (Ser/Thr) residues (O-linked). There are several variations in terms of glycan structures, which is translated in a wide range of biological functions (13, 14). Notably, terminal sugar sequences are among the features suggested as mediators of more specific roles (13). In this

From the [1]Priority Research Centre in Reproductive Science, School of Environmental and Life Sciences, University of Newcastle, Callaghan, NSW, Australia; [2]Centre for Chemical Biology and Clinical Pharmacology, Department of Biology, School of Environmental & Life Sciences, The University of Newcastle, Callaghan, Australia; [3]AgResearch, Grasslands Research Centre, Palmerston North, New Zealand; [4]Faculty of Pharmacy and Pharmaceutical Sciences, Monash University, NSW, Australia

*For correspondence: Mark A. Baker, Mark.Baker@newcastle.edu.au.

 DOI 10.1074/mcp.RA120.002109

context, sialic acid (Sia), a monosaccharide with a nine-carbon backbone and negatively charged, is considered an important terminal sugar.

The presence of Sia residues in glycoconjugates at the sperm surface seems to be vital for the success of fertilization. Indeed, in both humans (15) and boars (16) with unexplained infertility or subfertility, a decreased affinity for the lectin wheat germ agglutinin (WGA) has been reported, suggesting either GlcNAc and Sia residues are lacking within these cells. Interestingly, surface Sia residues have also been shown to help sperm to survive and migrate inside the female reproductive tract by reducing their phagocytosis and antigenicity (17–19) and by helping them to penetrate the cervical mucus (20). During sperm capacitation, it has been suggested that Sia residues are shed from the surface of spermatozoa. In this context, studies using lectin binding (21–24), surface charge determination (25, 26) radiolabeling of terminal sialyl residues (27) and HPLC measurement following acid hydrolysis (28) have all indicated that surface sialoglycoconjugates are probably lost or modified when spermatozoa are incubated under capacitating conditions. One model that has been put forward is that the shedding of Sia residues may be triggered by the release of neuraminidases present at the sperm surface (28). If this is the case, then the presence of oviduct fluid components (22) heparin (23) and/or albumin (29) in the medium probably facilitate this release (28).

Despite the data that show changes in sperm sialylation content during capacitation, no single publication has ever looked at which proteins are sialylated in spermatozoa, *yet al.*one quantified their levels during capacitation. With this in mind, we used titanium dioxide (TiO_2) followed by peptide-N-glycosidase F (PNGase F) cleavage to search for *N*-linked Sia-containing peptides and to quantify them during *in vitro* capacitation of mouse sperm. In addition, we further studied both mitochondrial aconitate hydratase (aconitase; ACO2) and endothelial lipase (EL) proteins to demonstrate a biologically meaningful effect of the Sia residue during sperm capacitation.

MATERIALS AND METHODS

Materials—Chemicals were purchased from Sigma-Aldrich at highest research grade except for the following products. Chloroform was purchased from Fronine (Riverstone, NSW, Australia). The 2-D quant kit was from G.E. Healthcare (Castle Hill, NSW, Australia). BCA assay kit was from Quantum Scientific (Milton, QLD, Australia). HEPES was from Invitrogen Australia (Melbourne, VIC, Australia). Sequencing grade trypsin was supplied by Promega (Alexandria, NSW, Australia). Antarctic phosphatase and PNGase F were purchased from New England Biolabs (Arundel, QLD, Australia). Phospholipase A_1 selective substrate (PED-A_1) (N-((6-(2,4-DNP)Amino) Hexanoyl)-1-(BODIPY® FL C5)-2-Hexyl-Sn-Glycero-3-Phosphoethanolamine) was purchased from Molecular Probes (Melbourne, VIC, Australia). The TiO_2 was collected from a disassembled column. Ionophore A23187 was purchased from Calbiochem (EMD Biosciences, La Jolla, CA). ANTIBODIES anti-phosphotyrosine PT66 (sigma, NSW Australia), Anti alpha Tubulin, anti-endothelial lipase and anti-aconitase were all form Abcam (Melbourne, Australia).

Sperm Collection and in Vitro Capacitation—Animal use was approved by institutional and New South Wales State Government ethics committees. Adult Swiss mice (~8–10 weeks) were euthanized and the epididymides were removed. Sperm cells were recovered from the cauda of the epididymides using retrograde flushing (30, 31) and then incubated for 10 min at 37 °C in 0.3% BSA BWW media (95 mM NaCl, 4.6 mM KCl, 1.7 mM $CaCl_2$, 1.2 mM KH_2PO_4, 1.2 mM $MgSO_4$, 25 mM $NaHCO_3$, 5.6 mM glucose, 0.27 mM sodium pyruvate, 44 mM sodium lactate, 20 mM Hepes, 5 U/ml penicillin, 5 mg/ml streptomycin; pH 7.4) to allow cell dispersion (32). For those cells undergoing capacitation, pentoxifylline and dibutyryl-cAMP (dbcAMP) were added group at a final concentration of 1 mM each. For the noncapacitated group, sodium bicarbonate was replaced by sodium chloride in the BWW media. All samples were incubated for 60 min at 37 °C and then sperm cells were washed three times (300 × *g*, 3 min) using BWW media without BSA.

Protein Extraction and Sialoglycopeptide Enrichment—Sperm pellets were resuspended in a lysis buffer consisting of 1% (w/v) C7BzO [3-(4-Heptyl) phenyl-3-hydroxypropyl) dimethylammoniopropanesulfonate], 7 M urea, 2 M thiourea, and 40 mM Tris (pH 10.4) at a final concentration of ~2.5×10^6/100 μL and incubated for 1 h (4 °C) with constant rotation. Supernatant (18,000 × *g*, 15 min, 4 °C) was recovered and total protein was quantified using a 2-D quant kit following manufacture's protocol. Proteins were reduced (10 mM DTT, 30 min, 30 °C), alkylated (45 mM iodoacetamide, 30 min, 30 °C) and 250 μg of protein was precipitated using methanol and chloroform (33). Samples were incubated overnight (37 °C) with trypsin at a 1:50 (trypsin/protein) ratio. Proteases were inactivated (bath sonication, 15 min) and peptides were treated with alkaline phosphatase (20 U, 2 h, 30 °C).

Enrichment of glycopeptides containing terminal Sia was performed as previously described (34). In brief, peptide samples were diluted in loading buffer [1 M glycolic acid, 80% (v/v) ACN, 5% (v/v) TFA] and then applied to TiO_2 beads (2 mg). After incubation for 1 h, TiO_2 beads were washed [washing buffer 1; 80% (v/v) ACN, 1% (v/v) TFA, and washing buffer 2; 20% (v/v) ACN, 0.1% (v/v) TFA] and dried in a vacuum concentrator. Enzymatic deglycosylation of *N*-linked sialoglycopeptides was performed with 1 μL of PNGase F for 3h at 37 °C. Released peptides were recovered, dried, resuspended in 0.1% (v/v) TFA and then loaded on a LC–MS (AmaZon ETD Ion Trap; Bruker Daltonik, Bremen, Germany) with an online-nanosprayer, and run as previously described (35).

Experimental Design and Statistical Rationale—Acquired CID spectra were processed in DataAnalysis 4.0; deconvoluted spectra were further analyzed with BioTools 3.2 software and submitted to Mascot database search (Mascot 2.2.04, Swissprot database (546439 sequences; 194445396 residues, release date 19/20/14)). The following variable modifications have been used: phosphorylation (STY), carbamidomethylation (C), deamidation (NQ) and oxidation (M). MS tolerance was set to 1.2 Da, whereas MSMS was set to 0.7 Da. Only one missed cleavage was allowed. To identify *N*-linked glycosylation sites, a deamidated Asn residue had to be flanked by the glycosylation consensus motif (NXS/T, where X is any amino acid besides proline) that was manually validated. Peptides that were assigned a deamidation event based solely on the MS data (*i.e.* no *y*- or *b*- fragment ion for a particular deamidated Asn residue could be detected) were presumed to be glycosylated only if a canonical N-glycan motif was present.

The derived MS datasets on the 3D-trap system were combined into protein compilations using the ProteinExtractor functionality of Proteinscape 2.1.0 573 (Bruker Daltonics, Bremen, Germany). To exclude false positive identifications, peptides with Mascot scores

below 40 were rejected. Peptides with a mascot score above 40 were manually validated in BioTools (Bruker Daltonics, Bremen, Germany) on a residue-by residue basis using the raw data to ensure accuracy as previously described (34).

MS-based label-free quantification of the N-glycopeptides identified was performed using the software Data Analysis 4.1 (Bruker Daltonik GmbH, Bremen, Germany). Peptides were matched based on charge state, m/z value and elution time. The match was confirmed by visual inspection of the peptide on the survey view and by manual comparison of the MS/MS spectra if available. Relative peptide quantification was carried out by integrating the area of the extracted ion chromatograms (XIC) of the monoisotopic peak from MS spectra (34). For peptide quantification, four biological replicates, each consisting of pooled samples from 3–4 mice, were run.

The data obtained by MS-based label-free quantification were normalized among runs using the average area of five different glycopeptides visually selected based on their quality and constant intensity. The normalized area of each glycopeptide was then compared between noncapacitated and capacitated sperm samples using student's *t* test. Relative immunoreactivity for EL and α-tubulin and sperm PLA_1 activity were compared among groups using paired *t* test. P-values < 0.01 were considered as significant. Standard errors are shown in the graphs. The data for acrosome reaction from 5 biological replicates were subjected to analysis of variance (two-way ANOVA) followed by paired *t* test. Data are shown as mean $\pm$ S.D. when not specified otherwise.

PLA_1 Activity Assay—The phospholipase A_1 (PLA_1) activity of EL in intact mouse spermatozoa was analyzed using a dye labeled-PLA_1 specific substrate (Molecular Probes, Melbourne, Australia) (36). The PLA_1 substrate is conjugated with a 4,4-difluoro-4-bora-3a,4a-diaza-*s*-indacene (BODIPY) fluor at the sn-1 position of the fatty acyl chain and with a dinitrophenyl group at the phospholipid head. The latter quenches the BODIPY fluor. However, when PLA_1 promotes the hydrolysis of the substrate, the distance created between the fluor and the quencher allows the emission of fluorescence.

Sperm samples were divided into six groups, which included (1) noncapacitated control, (2) noncapacitated supplemented with H89 or with (3) A23187, (4) capacitated control, and (5) capacitated supplemented with H89 or with (6) A23187. The compound H89 (10 μM final concentration) was supplemented 10 min prior to the addition of pentoxifylline and dbcAMP. After capacitation for 1h, ionophore A23187 was added to cells (20 μM final concentration) after 30 min of incubation and then samples were allowed to incubate for another 30 min. Spermatozoa were washed (300 $\times$ *g*, 3 min) twice using BWW media with BSA and then once with BWW media without BSA. Sperm pellets were then resuspended in BWW media without BSA to a final concentration of 20×10^6 sperm/ml.

A stock solution of PED-A_1 substrate (5 mM in DMSO) was diluted (1:625) with BWW medium without BSA yielding a final concentration of 8 μM. Aliquots of 25 μL of the PED-A_1 working solution were placed in a v-bottom 96-well plate and then 25 μL of the sperm samples was added. Controls included wells containing only PED-A_1 solution or sperm cells. The plate was incubated at 37 °C and fluorescence measurements were taken every 30 s during a 1h-period using the microplate reader FLUOstar OPTIMA (BMG Labtech, Mornington, VIC, Australia) with excitation and emission wavelengths of 485 and 510 nm, respectively. Linear regression was calculated using the average results for the first 10 min of reading and reaction rates (slope) were calculated for each sample. PLA_1 activity was assessed in five independent experiments.

Aconitase Vectors—ACO2 cDNA was ligated into the pcDNA3-EGFP plasmid. Primers were designed to have HindIII (forward) and NotI (reverse) restriction sites as well as 8 extra base pairs on the ends to allow enzyme cleavage. Two different reverse primers were used to create two different plasmids, the first containing a linker sequence to create an ACO2-EGFP fusion, and the second containing a linker sequence followed by a $(His)_6$-tag and stop codon to create his-tagged ACO2. This was achieved using mouse cDNA and the following overhanging primers:

Forward: ACGAATTC–AAGCTT–ATGGCGCCTTACAGCCTCCTGGT

Reverse 1: GGTGCTTA–GCGGCCGC–GAGCTTCCACCACCTCC–CTGCTGCAGCTCCTTCATCCTGTTG

Reverse 2: GGTGCTTA–GCGGCCGC–TCA–ATGGTGGTGGTGAT-GATGGCTTCCACCACCTCC–CTGCTGCAGCTCCTTCATCCTGTTG

For PCR, Thermo Scientific Phusion High-Fidelity DNA Polymerase was used, and their instructions followed. Each 20 μl PCR was made up with the following concentrations: 1 $\times$ HF buffer, 200 μM dNTPs, 0.5 μM each of forward and reverse primer, ~100 ng DNA, 3% DMSO and 1 unit Phusion polymerase. PCR conditions were: 98 °C for 30 s, [98 °C for 10 s, 65 °C for 30 s, 72 °C for 2 min] $\times$ 35 cycles, 72 °C for 10 min. Annealing temperature was optimized at 65 °C for both sets of primers.

PCR inserts and pcDNA3-EGFP vector were digested with Promega enzymes; NotI and HindIII after Wizard mini-prep kit clean-up. Insert and vector were ligated at a 3:1 ratio using Promega T4 DNA ligase and then transformed into *E. coli* cells on ampicillin agar plates. Singles colonies were cultured the following day and then plasmids extracted. Plasmids were again digested with HindIII and NotI to check for insertions and the ones containing inserts were sent away for Sanger sequencing using four sequencing primers to cover entire insert and check for mutations: GGACTTTCCA-AAATGTCG, AGGCCGAACAGACATTGC, AGATGCAGACGAGCTTCC, TTCATCCAGTGGACAAGC.

Site Directed Mutagenesis—To mimic the negative charge of the Sia modification on ACO2, we changed the amino acid Asparagine (N) 612 to Aspartic acid (D) using site directed mutagenesis. A single base pair change on chr15:81913178 to change the codon from AAC to GAC was achieved using the following primers:

Forward: TGCTCATCGGTGCCATCAACATC

Reverse: GGTTGTTAGAGATGTCATCCAGATGCCCAC

Phusion DNA Polymerase PCR was done using the same reaction as written in the above methods and the PCR conditions as follows: 98 °C for 3 min, [98 °C for 10 s, 64 °C for 30 s, 72 °C for 6 min] $\times$ 35 cycles, 72 °C for 10 min. Following PCR, the plasmid bands were cut out of an agarose gel, purified and digested with DpnI from NEB. Following another clean-up step, the plasmids were transformed into *E. coli* and grown on agar plates overnight. Single colonies were selected the following day and cultures grown overnight. Plasmids were extracted from these colonies and sent away for sequencing to check for mutation using sequencing primer AGATGCAGACGAGCTTCC.

Transfection—HEK293T cells were used for transfection with ACO2-EGFP plasmid and ACO2-$(His)_6$ plasmid including the WT and N612D versions of these plasmids. We confirmed that human cells would be suitable for transfection with the mouse ACO2 gene because of almost identical sequences. Cells were split into 6-well plates to attain ~50% confluence the following day. Transfection was done with 5 μg plasmid DNA and 10 μg PEI in 3 ml media. First, 5 μg of plasmid and 10 μg PEI were put into separate tubes and 150 μL DMEM (no FBS) added to each one. These were then mixed and incubated for 30 min. Next, media in the 6-well plates was replaced with 2.7 ml of fresh DMEM and the 300 μL DNA:PEI mix added. Cells were left to transfect for the times indicated and then harvested. ACO2-GFP cells were fixed using 4% paraformaldehyde for microscopy and FACS analysis or frozen at −80 °C for immunoblotting. ACO2-$(His)_6$ cells were frozen at −80 °C for immunoblotting or Aconitase assay.

Aconitase Assay—Aconitase assay from BioVision was used with adjusted methods.

To measure activity, we allowed aconitase to convers citrate into isocitrate, which was then coupled directly to a colorimetric assay allowing an absorbance readout.

Day 1: Frozen transfected HEK293T cells consisting of $(His)_6$-WT ACO2 transfected (WT), N612D mutant and control nontransfected cells were thawed on ice. Cells were resuspended in 400 ml lysis buffer (PBS pH 8, 10 mM imidazole, 0.5% tween) and then sonicated and centrifuged (16,000 g, 4 °C) for 15 min. A 200 μL aliquot of N612D and control samples were placed in fresh tubes and the rest discarded. The WT samples were split into 3 tubes: 200 μL, 100 μL and 50 μL. A 200 μL of lysis buffer and then 50 μL Ni-NTA agarose beads were added and samples rolled for 1 h at 4 °C. Beads were washed thrice in wash buffer (PBS pH 8, 20 mM imidazole, 0.5% tween) and once in kit assay buffer. Afterward, beads were resuspended in 100 μL kit assay buffer, 10 μL activation solution was added, and samples were rolled for 1 h at 4 °C. One hundred μL of reaction mix was added to each tube and samples rolled at room temperature overnight.

Day 2: Frozen non- and capacitated sperm cells were thawed on ice. Cells were resuspended in 100 μL kit assay buffer, sonicated and centrifuged (16,000 g; 4 °C) for 15 min. Ten μL of activation solution was added and samples incubated for 1 h on ice. Afterward, 100 μL reaction mix was added to each tube and samples incubated at room temperature for 2.5 h. Standards were made according to instructions and allowed to incubate for 30 min. The beads from day-1 preparation were centrifuged and, together with the non- and capacitated sperm prepared on day 2, were loaded in a 96-well plate in 100 μL duplicates. Ten μL of developer was added, samples incubated at room temperature 25 °C and read at 450 nm.

Following kit, nickel bead enrichment, $(His)_6$-recombinant protein were eluted with 250 mM imidazole and then frozen along with non- and capacitated samples. For immunoblotting, samples were methanol/chloroform precipitated and lysed in SDS-PAGE buffer.

SDS-PAGE and Immunoblotting—Noncapacitated and capacitated mouse spermatozoa (with and without H89) were prepared as described above and then diluted in SDS-PAGE buffer. Protein (10 μg) was separated by SDS-PAGE using 4-20% precast polyacrylamide gels (NuSep Ltd, Lane Cove, NSW, Australia) and then transferred onto nitrocellulose membrane Watman® Optitran® BA-S 85 (GE Healthcare, Castle Hill, NSW, Australia). The membrane was blocked with 3% BSA in TBS-T (1 h at room temperature) and incubated overnight at 4 °C with rabbit polyclonal antibody raised against EL (orb100394, LIPG; Biorbyt) at a dilution of 1:500 in 5% (w/v) skim milk TBS-T (0.02 M Tris, 0.15 M NaCl, 0.1% (v/v) Tween-20; pH 7.6).

After three washes, membrane was incubated for 1 h at room temperature with anti-rabbit IgG horseradish peroxidase (HRP) conjugate (Sigma-Aldrich) at a concentration of 1:1000 in 5% (w/v) skim milk TBS-T. The membrane was washed thrice, and immunoreacted proteins were detected using an enhanced chemiluminescence (ECL) kit (Amersham Pharmacia Biotech International) according to the manufacturer's instructions.

To confirm the capacitation of sperm cells and the efficiency of H89 at inhibiting tyrosine phosphorylation via PKA, samples were probed with the mouse monoclonal anti-phosphotyrosine–peroxidase antibody PT66 at 1:2000 (A5964; Sigma-Aldrich).

Immunoblots of WT and mutant ACO2 were essentially performed as previously described (35). The following antibody dilutions were used: rabbit polyclonal anti-Aconitase 2 antibody at 1:1000 (ab83528; Abcam), rabbit polyclonal anti-6 × His tag antibody at 1:1000 (ab1187; Abcam). Anti-GFP was a kind gift from Peter Lewis and used at 1:1000. All secondary antibodies were used at a 1:1000 dilution. Equal loading was confirmed by stripping the membrane and then reprobing it with a mouse monoclonal anti-α-tubulin antibody at 1:4000 (T5168; Sigma-Aldrich).

Immunocytochemistry—Capacitated and noncapacitated intact mouse spermatozoa were fixed in 4% (w/v) formaldehyde for 10 min at room temperature. Cells were washed three times in PBS containing 0.5 M glycine, immobilized on poly-L-lysine coverslips and permeabilized with ice cold methanol for 10 min. Coverslips were washed, blocked for 1 h with 3% (w/v) BSA in PBS and incubated overnight with anti-EL antibody in a 1:50 dilution with PBS containing 1% (w/v) BSA. Following three washes with PBS, cells were incubated with Alexa Fluor® 488 goat anti-rabbit IgG (Life technologies) in a 1:100 dilution with PBS containing 1% (w/v) BSA. Coverslips were washed as described above and then mounted with Mowiol antifade medium. Cells were evaluated using phase contrast and epifluorescence microscopy.

Acrosomal Status—The acrosomal status of mouse spermatozoa was assessed either at time 0 (noncapacitated) or following 30 min of capacitation (37 °C; 5% CO_2). After 30 min of incubation, the ionophore A23187 (10 μM final concentration in DMSO) or DMSO vehicle only were added and then cells were incubated for 30 min. Samples were washed twice using PBS and 10 μl of sperm suspension was spotted onto superfrost slides, spread with a glass pipette and air-dried. Slides were immersed in absolute methanol for 15 min, rinsed with PBS and then incubated for 30 min with FITC-conjugated *Arachis hypogaea* peanut agglutinin (FITC-PNA) (15 μg/ml final concentration). The slides were rinsed in PBS and mounted with antifade media. For each slide, images of adjacent fields were recorded under a × 40 magnification to achieve a sperm count of at least 100 spermatozoa. Spermatozoa were classified into one of the three categories of FITC-PNA labeling: I = intact acrosome; II = partial acrosome reaction; and III = complete acrosome reaction. For each experimental condition, a minimum of 3 slides were examined and quantified.

Molecular Modeling; Covalent Docking Model of Sialic Acid Binding of N612 to Aconitate Hydratase—Molecular docking experiments were carried out using the program GOLD (Genetic Optimization for Ligand Docking) version 5.2 and favoring the CHEMPLP Scoring system (Verdonk 2003). The three-dimensional iteration of Sialic acid (MolPort-008-267-866) was used for covalent docking onto the identified target residue of N612 on a model of Aconitate hydratase, mitochondrial precursor from *Mus musculus* (EC: 4.2.1.3) generated by the PHYRE2 protein recognition server Kelley (2015). The size of the search domain was set to 10 Å and the covalent docking function within GOLD was employed. Docking was executed using a 100% search efficiency, generating ten Genetic Algorithm (GA) runs, whereas the rotameric states of several sidechains including Gln563, Lys605 and Arg648 were set to library rotamer orientations and the remainder of the site remained rigid. The generated binding poses were then inspected, and conformations were chosen for further analysis considering their ranking and interactions with the probed residues. Molecular visualizations were performed using the software package PYMOL (Schrödinger, NY).

RESULTS

To determine the efficiency of the protocol used here to induce sperm capacitation, tyrosine phosphorylation was measured (Fig. 1). As shown, tyrosine phosphorylation increased during capacitation, which could be abrogate with the PKA inhibitor H89, suggesting that the sperm cells used in this study were capacitating. The experimental paradigm used in this study was to compare the changes associated with the capacitation process

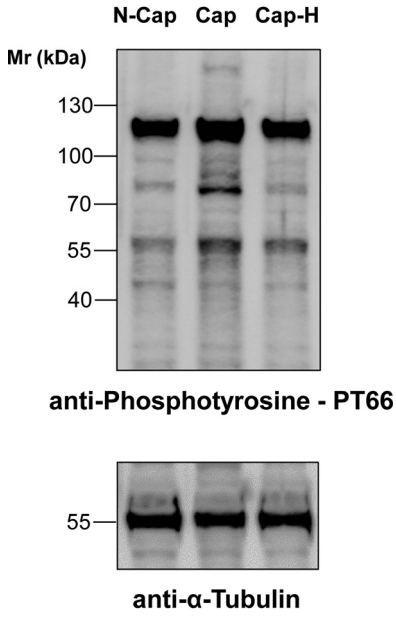

FIG. 1. Immunoblotting of mouse cauda sperm incubated in noncapacitating (N-Cap) or capacitating media supplemented (Cap-H) or not (Cap) with the PKA inhibitor H89. Protein extraction was performed in SDS-PAGE buffer and 10 μg was loaded per lane. Membranes were probed with anti-Phosphotyrosine PT66 antibody and then re-probed with anti-α-tubulin. The data show one replicate that has been repeated in 6 biological replicates.

itself (Cap *versus* Cap-H, Fig. 1) as opposed to changes over time (N-Cap *versus* Cap, Fig. 1).

Sialylated Glycoproteins Identified in Mouse Sperm—The protocol to enrich for sialylated *N*-linked glycopeptides is shown in Fig. 2. Herein, spermatozoa were obtained from the mouse epididymides, combined, and then separated into two separate tubes. Although one tube had capacitating media, the other lacked sodium bicarbonate, which is essential for this process. The samples were washed, lysed, and digested. Sialylated-glycoprotein enrichment was performed using TiO_2 beads. Although this is not specific for glycopeptides, but rather for negatively charged molecules, the elution through PNGase F treatment of the beads allows the selection of *N*-linked glycopeptides generally or sialylated glycopeptides specifically.

Enrichment of sialylated *N*-linked glycopeptides using TiO_2 allowed the identification of 142 unique peptides, which were from 90 different glycoproteins (Table I), demonstrating that some proteins possessed *N*-linked glycopeptides with terminal Sia in more than one position. Of interest, the characterization of the glycopeptides containing Sia residues represented 36.7% of the total nonreductant peptides identified by MS/MS. This is in perfect agreement with our previous paper with rat sperm, in which around 34% of the peptides identified were classified as glycopeptides after enrichment using TiO_2 (34).

Because of ion fragmentation patterns (*i.e.* no visualization of the *y*- or *b*- fragment ion for the deamidated Asn), a

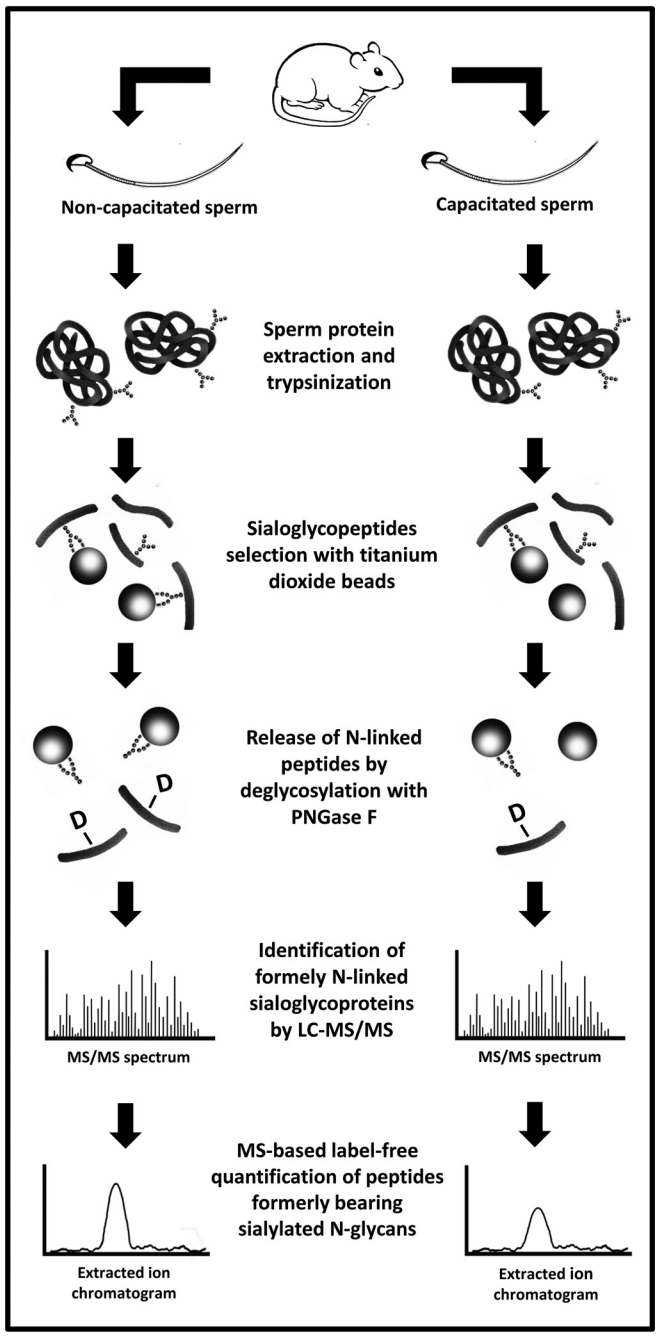

FIG. 2. Schematic representation of the strategy used to identify and quantify sialylated *N*-linked glycopeptides extracted from mouse sperm. Sperm cells retrieved from mouse epididymides were divided into two groups: one incubated in capacitating conditions (supplemented with 1 mM pentoxifylline and 1 mM dibutyryl-cAMP) and the other in noncapacitating conditions (without supplementation and sodium bicarbonate). Sperm proteins were recovered and digested (trypsin). Sialylated-glycoproteins were enrichment using TiO_2 beads. The *N*-linked glycopeptides were eluted from the beads after PNGase F treatment and then identified and quantified using LC–MS/MS and label-free techniques. "-D" represents deamidates asparagine.

TABLE I

List of sialylated N-glycopeptides identified in non-capacitated and capacitated mouse sperm and their regulation during the process of capacitation

Protein ID	Peptide Sequence	Mascot Score	Fold Change	*p* value	MS/MS (suppl 1)
Angiotensin-converting enzyme	K.EADNFFTSLGLLPVPPEFW**NK.S**	42.9	ND	ND	1
	K.LITGQP**NMS**ASAMMNYFKPLTEWLVTENR.R*	40.7	ND	ND	2
	K.STEVS**NHT**LK.Y	54.0	−1.09	0.063	3
	K.TFDVSNFQ**NSS**IK.R	76.9	−1.34	0.074	4
Aconitate hydratase, mitochondrial precursor	R.GHLD**NIS**NNLLIGAINIENGK.A*	67.8	2.04	0.016	5
Acrosin precursor	R.VDLIDLDLC**NST**QWYNGR.V	128.0	−1.15	0.113	6
ADAM 26A	R.KEKNECDLPEWC**NGT**SAECPGDVYK.A	80.8	−1.32	0.243	7
ADAM 24	K.LS**NCS**YEVLWAHMI**NK.S**	49.5	ND	ND	8
ADAM 2 precursor	R.AFS**NCS**MEDFSK.F	85.7	ND	ND	9
	R.**NTT**DYVGATYQGK.M	56.0	ND	ND	10
ADAM 5	K.A**NLS**VAYAQIR.D	80.8	1.09	0.314	11
ADAM 1b	K.EGDVCRPADGPCDLEEYC**NGT**SAACPSDR.K	82.6	−1.52	0.081	12
Anthrax toxin receptor-like	K.DFYQV**NIS**GHGL**NNT**SNMK.Q*	62.2	1.53	0.162	13
Beta-2-glycoprotein 1 precursor	K.DYRPSAG**NNS**LYQDTVVFK.C	59.2	1.12	0.264	14
	K.**NIS**FACNPGFFL**NGT**SSSK.C*	116.5	2.06	0.163	15
Sodium/potassium-transporting ATPase subunit beta-3	K.EE**NAT**IATYPEFGVLDLK.Y	85.2	−1.27	0.162	16
Basigin precursor	K.SQLTISNLDVNVDPGTYVC**NAT**NAQGTTR.E*	63.4	1.19	0.063	17
	K.TSDTGEEEAIT**NST**EANGK.Y	151.1	−1.35	0.090	18
Bactericidal permeability-increasing protein	K.T**NAS**LEVDAEENR.L	92.0	−1.27	0.214	19
C4b-binding protein	K.ALCQKPEVG**NGT**LSDEK.D	52.8	−1.30	0.233	20
	R.CEQEASEDLKPALTG**NK.T**	43.1	ND	ND	21
	R.LACL**NGT**VLR.G	76.8	−3.62	0.009	22
Carbonic anhydrase 4 precursor	R.Y**NGS**LTTPNCDETVIWTVYK.Q	88.6	1.71	0.088	23
Carboxypeptidase A5 precursor	K.AGFGG**NGS**NKNPCSETYR.G*	40.3	ND	ND	24
Carboxypeptidase Q	K.EVMNLLQPL**NVT**K.V	80.1	1.43	0.266	25
CD109 antigen homolog precursor	R.FLVTAPGIIRPGA**NVT**IGVDLLENSPPQVLVK.A*	51.9	−2.03	0.084	26
CD151 antigen	K.LQQEFHCCGS**NNS**QDWQDSEWIR.S	85.7	−1.03	0.466	27
CD59B glycoprotein	K.I**NTT**CSPNLDSCLYAVAGR.Q	89.4	1.02	0.466	28
Clusterin precursor	K.AFPEVC**NET**MMALWEECKPCLK.H*	46.9	−2.55	0.164	29
	R.QEL**NDS**LQVAER.L	72.9	ND	ND	30
Choline transporter-like protein 5	R.CIPDLSAL**NGT**WTPGSR.M	84.3	1.11	0.312	31
Cation channel sperm-associated protein subunit gamma 2	K.LY**NMS**GDYGIPDLFFLDK.G	63.9	−1.30	0.163	32
	R.GVD**NST**YCDYK.L	73.8	ND	ND	33
Cation channel sperm-associated protein subunit beta	K.TPVYNPLGL**NLT**IQGSELFHFK.V*	66.5	ND	ND	34
CUB and zona pellucida-like domain-containing protein 1 precursor	K.ALVLQLSANE**NCT**WTIERPE**NR.S** *	122.2	−1.72	0.181	35
	K.GFSASYTSIYIHDV**NTT**SLSCVSDK.M	89.8	1.77	0.146	36
Dickkopf-like protein 1 precursor	K.VTD**NQT**GEVLISEK.V	79.2	1.04	0.460	37
Dipeptidase 3 precursor	R.HHFYT**NIS**GLTSFGEK.V	101.5	−1.30	0.122	38
	R.MCSAYPELELVTSADGL**NNT**QK.L	150.4	−1.08	0.434	39
Embigin precursor	K.K_DDEPLETTGDF**NTT**K.M	75.9	1.42	0.338	40
	K.YII**NGS**HA**NET**R.L	68.4	ND	ND	41
Endoplasmin precursor	K.HN**NDT**QHIWESDSNEFSVIADPR.G*	93.0	−3.89	0.200	42
	R.TDDEVVQREEEAIQLDGL**NAS**QIR.E	85.2	ND	ND	43
Equatorin	K.AV**NET**AVSMDDK.D	96.8	−1.29	0.145	44
	K.DQFFQPIPASDL**NAT**NEDK.L	101.8	1.23	0.241	45
Carboxylesterase 5A	K.HDLQVVANVCDC**NVS**DSK.A	103.1	−1.43	0.323	46
Interferon-induced guanylate-binding protein 1	K.LQEQERLLKQGFQ**NES**LQLR.Q	42.0	−1.22	0.201	47
Glycerophosphodiester phosphodiesterase domain-containing protein 4	K.EVLPSAAG**NHT**SNF**NWT**FLSTLNAGK.W*	91.7	−1.02	0.469	48
Gamma-glutamyltranspeptidase 1 precursor	R.LA**NTT**MF**NNS**K.D	56.2	ND	ND	49
Gamma-glutamyltransferase 7	R.TA**NHS**APSLENSVQPGK.R	49.2	ND	ND	50
Beta-galactosidase-1-like protein	R.CGSLQGLYTTIDFGPAD**NVT**R.I*	45.6	ND	ND	51
Solute carrier family 2, facilitated glucose transporter member 3	K.DFL**NYT**LEER.L	69.6	−1.10	0.271	52

TABLE I—*continued*

Protein ID	Peptide Sequence	Mascot Score	Fold Change	*p* value	MS/MS (suppl 1)
Hexokinase-1	K.SQ**NVS**MESEVYDTPENIVHGSGSQLFDH-VAECLGDFMEK.R*	94.2	ND	ND	53
Hyaluronidase PH-20 precursor	K.VG**NAS**DPVPIFVYIR.L	60.6	−1.53	0.102	54
Hypoxia up-regulated protein 1	R.AEPPL**NAS**AGDQEEK.V	61.0	−4.07	0.165	55
	R.VFGSQ**NLT**TVK.L	76.2	ND	ND	56
Izumo sperm-egg fusion protein 1 precursor	R.VWE**NSS**ETLIAK.G	85.7	−1.24	0.129	57
Casein kinase I isoform gamma-2	K.NQAL**NST**NGELNTDDPTAGHSNAPIAAPAEVE-VADETK.C*	92.2	−1.32	0.210	58
Laminin subunit alpha-1 precursor	K.LDELK**NLT**SQFQESVD**NIT**K.Q*	50.0	ND	ND	59
Lysosome-associated membrane glycoprotein 1 precursor	R.AF**NIS**P**NDT**SSGSCGINLVTLK.V*	61.4	−3.42	0.113	60
	R.L**NMT**LPDALVPTFSIS**NHS**LK.A*	65.8	ND	ND	61
Epididymal-specific lipocalin-8 precursor	K.AVY**NSS**GSCVTESSLGSER.D	109.7	−1.41	0.162	62
Endothelial lipase	K.DPEQEGC**NLS**LGDSK.L*	79.3	ND	ND	63
	K.IEL**NAT**NTFLVYTEEDLGDLLK.M	71.2	ND	ND	64
	K.LLENCGF**NMT**AK.T	62.7	−1.33	0.011	65
Lipid phosphate phosphohydrolase 1	K.I**NCS**DGYIEDYICQGNEEK.V	120.3	1.06	0.359	66
Leucine-rich repeat-containing protein 52 precursor	K.YVFA**NTT**SLR.Y	52.5	ND	ND	67
	R.L**NIS**HNPHLLYLDK.Y	40.6	ND	ND	68
Ly6/PLAUR domain-containing protein 4 precursor	K.FQAGNL**NTT**FLIMGCAR.D	118.3	1.14	0.299	69
	R.SYLCN**NLT**NLEPFVR.L*	76.6	−1.19	0.270	70
Lysosomal alpha-mannosidase	R.DDYRPTWTL**NQT**EPVAGNYYPVNTR.I*	49.0	ND	ND	71
Epididymis-specific alpha-mannosidase precursor	K.QFF**NAS**VQFDNMDPLLDYINQR.T*	57.0	−2.59	0.155	72
	K.Y**NLT**L**NDT**SIVHPVLWLMLGPK.S	89.7	1.23	0.243	73
Membrane cofactor protein precursor	K.**NGT**HTLTDINVFK.Y	54.3	1.05	0.384	74
Mitochondria-eating protein	R.DNSPDQDQHQSD**NES**FSETQPTQVQD-DLAESGK.S*	61.5	−1.69	0.127	75
Membrane metallo-endopeptidase-like 1	K.NGNMLDWWS**NFS**AR.H	63.0	−1.91	0.118	76
	R.EEMAEVLELETHLA**NAT**VPQEK.R	56.9	−1.24	0.362	77
	R.VLIDLFIWNDDQ**NSS**R.H	58.9	ND	ND	78
Ecto-ADP-ribosyltransferase 3	R.KGTSNDLVLQSI**NST**CSYYECAFLGGLK.T*	86.0	−1.18	0.320	79
	R.LG**NFT**LAYSAKPETADNQR.V*	112.9	1.19	0.079	80
Nicastrin	K.DLYEYSWVQGPWNS**NR.T***	45.9	ND	ND	81
L-amino acid oxidase precursor	K.VVTLGL**NR.T**	55.6	−1.34	0.138	82
	R.TLGL**NLT**QFTQYDENTWTEVHNVK.L	97.3	−1.10	0.418	83
Nuclear pore membrane glycoprotein 210-like precursor	K.CFP**NSS**VIEEDGGGLLR.S	99.7	−1.16	0.352	84
	K.EYFEEQLSTS**NGS**YHVVK.A	44.4	−1.90	0.069	85
	K.SS**NET**LAHFEDSK.S	83.2	−1.38	0.051	86
	R.EVVV**NAS**SR.L	58.7	1.01	0.470	87
	R.G**NST**ILAR.D	68.4	−1.78	0.179	88
	R.ILIPFIPGFYM**NQS**EFVLGHK.D	45.3	−1.05	0.467	89
	R.KFD**NFS**SLMLEWK.S	66.6	−1.10	0.315	90
Lysosomal Pro-X carboxyllpeptidase precursor	K.**NIS**SHSNIIFSNGELDPWSGGGVTR.D*	91.7	ND	ND	91
Protein disulfide-isomerase-like protein of the testis	K.ALLF**NNS**DEVADFVK.S	82.0	−2.69	0.235	92
Phospholipase B1, membrane-associated	K.AE**NLT**SQVR.T	73.6	1.11	0.268	93
	K.NSNLG**NGT**WMVCEER.A	89.7	−1.67	0.053	94
	K.TLE**NVT**TLPNILR.K	42.1	1.00	0.499	95
	R.D**NFT**VVVQPLFE**NVS**MPR.T*	58.5	ND	ND	96
	R.HSQ**NLT**AMQELK.K	78.2	−1.38	0.153	97
Putative phospholipase B-like 1	R.DQG**NVT**DMASMK.Y	89.4	−1.10	0.326	98
	R.F**NET**LHR.G	49.8	−1.23	0.200	99
Prominin-1 precursor	K.DALQ**NMS**SSLK.S	50.1	ND	ND	100
	K.SLQDAATQLNT**NLS**SVR.N	121.1	−1.46	0.244	101
Inactive serine protease 39	R.ILLGYNQLSNPS**NYS**R.Q	104.5	−2.00	0.001	102
Serine protease 42	K.LQHPV**NFT**TNIYPVCIPSESFPVK.A*	84.1	1.22	0.217	103
Serine protease 44	K.GGDACQGDSGGPLVCEF**NK.T**	97.1	−1.61	0.067	104
Serine protease 46	K.VGVQTLPD**NST**SELLVTR.I	100.3	1.15	0.349	105

TABLE I—*continued*

Protein ID	Peptide Sequence	Mascot Score	Fold Change	*p* value	MS/MS (suppl 1)
Serine protease 52	R.NCWVTGWGIT**NTS**EK.G	101.7	−3.09	0.003	106
Prostaglandin-H2 D-isomerase precursor	K.TVVAPSTEGGL**NLT**STFLR.K	141.6	−1.42	0.279	107
Patched domain-containing protein 3	K.VVQE**NGT**QILYQEVCAK.Y	94.7	1.14	0.192	108
	R.FVQGHFST**NDT**YR.F	60.9	−1.17	0.324	109
Pituitary tumor-transforming gene 1 protein-interacting protein precursor	R.VGCSEYT**NR.S**	59.5	−1.02	0.432	110
RING finger protein 126	R.NTE**NGS**APSTAPTDQNR.Q	75.4	ND	ND	111
Solute carrier family 13 member 5	R.AMFNLDNFPDWA**NST**SVNT.-	100.3	1.03	0.472	112
Solute carrier family 22 member 21	R.IPDTV**NLS**SAWR.N	91.2	−1.09	0.201	113
	R.LATIA**NFS**ELGLEPGR.D	96.2	−1.11	0.282	114
Sperm acrosome membrane-associated protein 1 precursor	K.LLKPDQQPVILT**NDS**AVLEITR.E	138.6	1.38	0.258	115
Saccharopine dehydrogenase-like oxidoreductase	K.ACIE**NGT**SCIDICGEPQFLELMHAK.Y	81.0	ND	ND	116
	R.NQM**NGT**LTAVESFLTINTGPEGLCIHDGTWK.S*	91.5	ND	ND	117
Sortilin precursor	R.HLYTTTGGETDFT**NVT**SLR.G	62.3	−2.18	0.053	118
Kunitz-type protease inhibitor 4	R.FFY**NQT**AK.Q	42.0	−1.09	0.317	119
Signal peptide peptidase-like 2B	K.SGNSIMVEVATGPS**NSS**THEK.L	87.6	1.18	0.290	120
Suppressor of G2 allele of SKP1 homolog	R.CQEIQ**NGS**ESEVSASQR.T	84.2	ND	ND	121
Synaptophysin-like protein 1	K.**NQT**VTATFGYPFR.L	89.3	−1.29	0.154	122
Testisin precursor	K.LSSPVTYNNFIQPICLL**NST**YK.F	94.7	−1.35	0.194	123
Testis-expressed sequence 29 protein	K.FAVCDIPLYDICDY**NVT**R.E	101.0	1.02	0.448	124
Transmembrane protease serine 12	R.EEG**NGT**TILQEAK.V	43.0	ND	ND	125
Testis-expressed protein 101 precursor	R.HCPTCVALGSCSSAPSMPCA**NGT**TQCYQGR.L	75.2	−1.99	0.004	126
	R.TF**NWT**SK.A	48.7	−1.91	0.001	127
	R.VPETTATS**NMS**GTR.H	93.3	−2.01	0.001	128
Ubiquitin carboxyll-terminal hydrolase 7	R.ITQNPVING**NVT**LSDGHSNAEEDMEDDTSWR.S*	109.5	ND	ND	129
Zonadhesin precursor	K.CPLGTECK_DSVDGGS**NCT**K.I	51.9	ND	ND	130
	K.DAQGDLIPA**NK.T**	74.4	−1.24	0.189	131
	K.DGSS**NCT**NIPLQCPAHSR.Y	93.0	−1.14	0.183	132
	K.FQCPSETYCK_DIEDGNS**NCT**R.I	43.0	ND	ND	133
	K.TCTTLCTCSAHS**NIT**CSPTACK.A	52.2	−1.04	0.236	134
	R.VGSQSSGWM**NSS**VTIPK.G	52.6	−2.06	0.009	135
Zona pellucida sperm-binding protein 3 receptor precursor	K.GVCLKPMVING**NLS**VER.V	63.8	1.58	0.191	136
	K.TYLFGHEE**NST**EHAMK.G	63.8	−1.64	0.137	137
	R.ASLNDPQTVTCQE**NLT**WSSTNGCER.I	137.3	−1.03	0.357	138
	R.LALFTFP**NIS**ET**NVTNK.T** *	95.9	1.27	0.191	139
	R.V**NSS**HLSCDE**NGS**WVYSTFCAR.K*	75.1	1.08	0.281	140
Zona pellucida-binding protein 1 precursor	R.DGTHCLQC**NNS**LVYGAK.T*	104.7	1.02	0.435	141
Zona pellucida-binding protein 2	K.GNSQI**NIT**NTGELVLK.D*	76.5	1.70	0.145	142

*ambiguous localization of deamidated residue.
Consensus sequence for N-glycosylation is shown underlined and in boldface.
Numbers in MS/MS column correspond to page in supplemental I which contains MS/MS spectrum of the glycopeptides.
ND (not determined) is used when the area under the curve could not be measured in all samples.

precise identification of the residue containing the deamidation was not possible in all cases. Hence, the peptides exhibiting ambiguous annotation of the deamidated residue are indicated in Table I with an asterisk. supplemental I contains MS/MS spectrum from all peptides present in Table I whereas supplemental II presents data such as measured m/z values, peptide charge and retention times.

Changes in Sialylated N-Linked Glycopeptides during Capacitation—The data for label-free quantification of the *N*-linked glycopeptides in noncapacitated *versus* capacitated sperm are shown in Table I. Some glycopeptides were presented at very low amount, impairing their quantification in some biological replicates. These cases are indicated in Table I as not determined (ND) because we were not confident to report these further. Of interest, nine (6.3%) of the glycopeptides identified here underwent significant changes during sperm capacitation. These glycopeptides belong to the proteins: ACO2, C4b-binding protein (C4BP), EL, inactive serine protease 39 (PRSS39, also known as testicular-specific serine protease 1; TESP1), serine protease 52 (PRSS52, also known as testicular-specific serine protease 3; TESP3), testis-expressed protein 101 (TEX101) and zonadhesin (Table I). Interesting, these glycopeptides were shown to be reduced during capacitation except for the peptide from ACO2, a protein involved in the tricarboxylic acid (TCA) cycle (Table I).

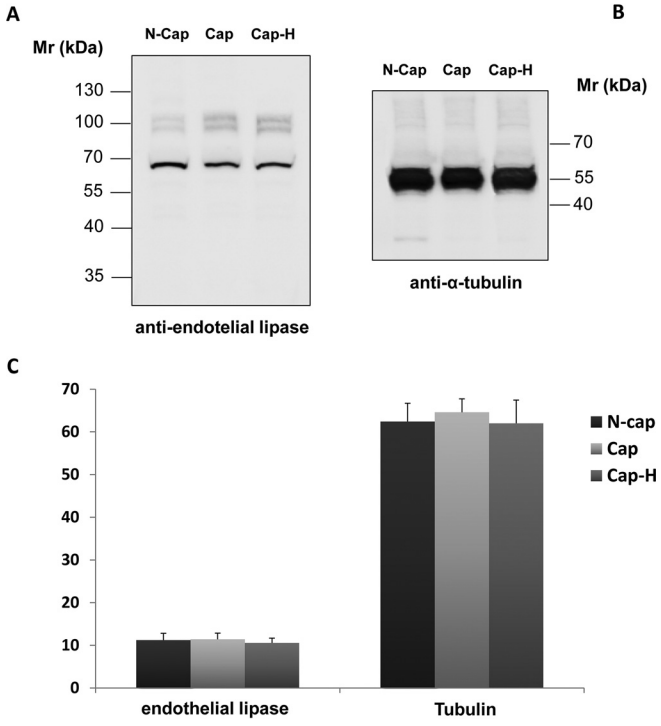

FIG. 3. Immunoblot analysis of cauda spermatozoa from mouse. Sperm samples were incubated in noncapacitating (N-Cap) or capacitating media supplemented (Cap-H) or not (Cap) with the PKA inhibitor H89. Extraction was performed using SDS-PAGE buffer and 15 μg of protein was loaded per lane. *A*, Membranes were probed with anti-EL and then (*B*) re-probed with anti-α-tubulin. *C*, Graphic below shows relative immunoreactivity levels of both EL (*left*) and α-tubulin (*right*). No statistically significant difference was observed among groups, which consist of five biological replicates each.

Determination of EL Amount and Sub-Cellular Localization—To determine the consequences of sialylation changes during capacitation, we choose two proteins for further study: the EL and ACO2. The EL has been reported as primarily having PLA_1 activity (37). This was of particular interest, because changes in the composition of lipids from cell membranes, such as the formation of lysophospholipids by phospholipids hydrolysis, are known to modify membrane fluidity (38, 39) and function through the modulation of receptors (40), channels (41, 42) and enzyme activity (43) within its structure. Considering that morphological and functional changes in sperm membranes, including alteration in membrane fluidity, are essential for capacitation (44) and that lysophospholipids may be involved in the modulation of the acrosome reaction (45), we further investigated the behavior of EL during this process.

Immunoblotting for EL was performed, aiming to determine what happens to the entire protein during capacitation. As shown in Fig. 3, the total amount and the molecular weight of EL did not change after capacitation (Fig. 3*A*, lanes 1 and 2). In addition, the use of the PKA inhibitor H89 during capacitation also did not affect the amount of EL (Fig. 3*A*, lanes 2 and 3). To demonstrate equal loading, we re-probed the sample with anti-α-tubulin antibody (Fig. 3*B*). Using the software Image J, the quantitative values of each band were plotted to confirm that no significant change occur in EL expression after capacitation (Fig. 3*C*).

To verify whether the protein EL is redistributed in spermatozoa during capacitation, we performed immunostaining using anti-EL antibody. Immunostaining for EL was observed in both head and tail regions of noncapacitated (Fig. 4*A*, 4*C*) and capacitated (Fig. 4*B*, 4*D*) mouse sperm. For both groups, the anterior acrosome region stained for EL whereas the equatorial region showed no staining. In addition, the staining intensity of the postacrosomal sheath showed high variation among cells; being absent in some cases (Fig. 4*B*, white arrow exemplifies this variation). In the tail region, although the midpiece and the cytoplasmic droplet showed high staining for EL, we noted that some cells exhibited weaker labeling of the midpiece (Fig. 4*C*, 4*D*). Of interest, the percentage of these cells, with reduced immunoreactivity for EL at the midpiece, increased when sperm was incubated in capacitating conditions (from around 7% to 68%). The same was observed in samples capacitated with the PKA inhibitor H89, suggesting that the diminish in EL immunofluorescence within the midpiece is independent of PKA (data not shown). Secondary only controls showed no fluorescence (Fig. 4*E*, 4*F*).

Loss in EL Activity Occurs during Capacitation, Independent of H89 and the Acrosome Reactions—To determine if the loss of Sia residue on EL affected enzyme activity, we specifically measured PLA_1 activity on both non- and capacitated spermatozoa. Furthermore, as the immunofluorescence showed quite a varied pattern of EL expression, including acrosome location, we wanted to see if the loss of the acrosome had any effect of the overall EL activity. Therefore, we incubated sperm under non- or capacitating condition, with and without H89. Second, both non- and capacitated spermatozoa were induced to undergo the acrosome reaction. These sperm cells were subsequently washed, then the level of intact, partial, or complete acrosome loss were measured using FITC-PNA staining. As shown in Fig. 5, capacitated sperm plus ionophore A23187 had the highest level of complete acrosomal loss as expected.

To determine whether a change in EL activity occurred during capacitation, we measured PLA_1 activity before and after capacitation, together with the inhibitor H89 or the acrosomal-inducer, ionophore A23187. We observed a significant loss in the PLA_1 activity of EL during capacitation (Fig. 6*A*, bars N-cap *versus* Cap). An example of the loss in PLA_1 activity is demonstrated in Fig. 6*B*. Here, two of the five biological replicates are shown over time from either noncapacitated (solid line) or capacitated (dotted line) sperm populations. Addition of the PKA inhibitor H89, which is commonly used to prevent capacitation, failed to abrogate the loss of PLA_1 activity (Fig. 6*A*, N-cap + H89 *versus* Cap + H89).

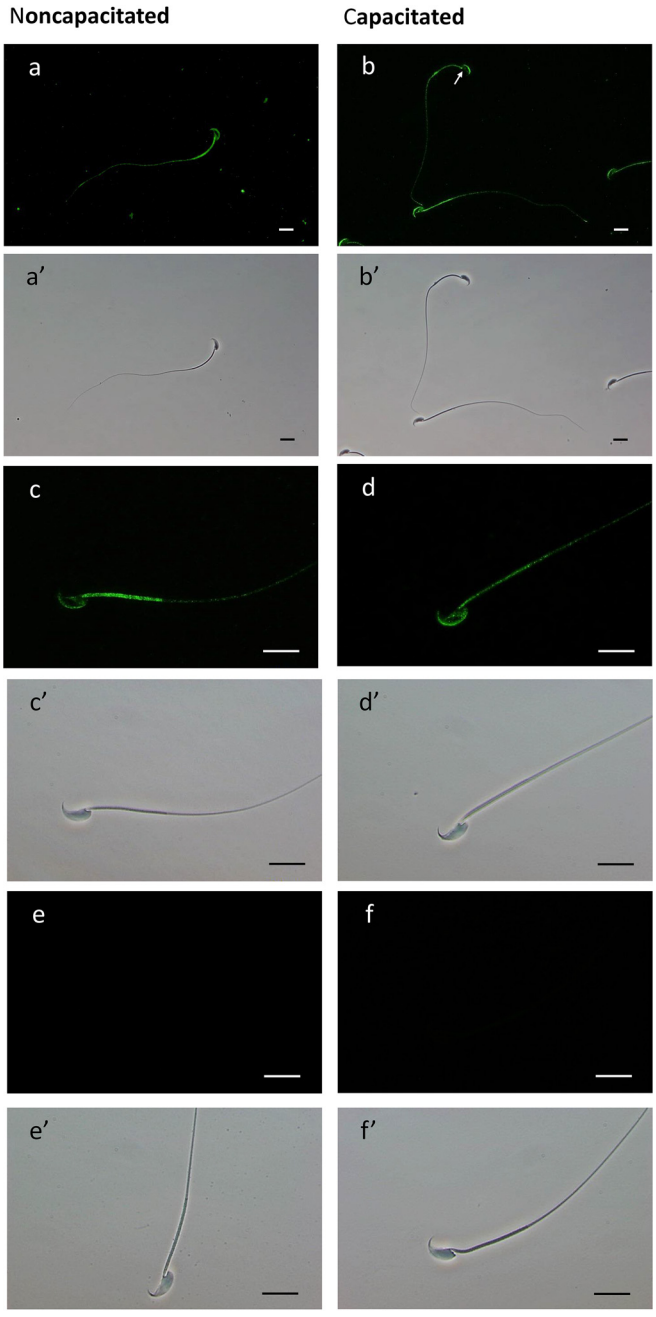

FIG. 4. Immunofluorescent localization of EL and the corresponding phase-contrast micrographs of noncapacitated and capacitated mouse sperm cells. (*A–D′*) Fixed spermatozoa were immobilized on pre-coated slides, permeabilized with ice cold methanol and incubated overnight with anti-EL antibody. Alexa Fluor 488-conjugated secondary antibody was used for detection of the primary antibody. Primary antibody was omitted in control (*E* and *F*). The scale bars represent 20 μM. The experiment was repeated using four biological replicates.

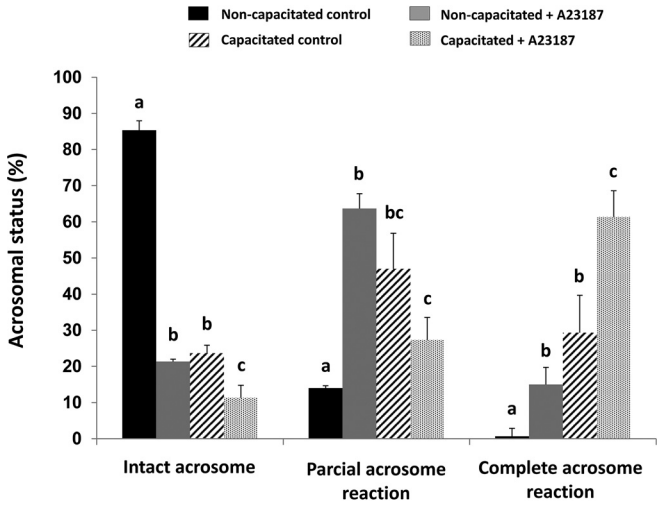

FIG. 5. Assessment of acrosomal status by FITC-PNA labeling of noncapacitated (*black* and gray bars) and capacitated (hatched and dotted bars) mouse sperm either with (grey and dotted bars) or without (*black* and hatched bars) previous incubation with calcium ionophore A23187. Sperm were counted for intact, partial or complete acrosome reaction. The data were expressed as mean ± S.E. Different letters represent statistical differences ($p < 0.01$) between treatments within each category (intact, partial or complete acrosome reaction). The graph represents the average of 5 biological replicates.

Furthermore, the loss of the acrosome had no further bearing on the reduction of the PLA_1 activity in EL, with acrosome-reacted capacitated spermatozoa (Fig. 6*A*, bar Cap + A23187) having a similar activity to the capacitated (Fig. 6*A*, bar Cap) and the H89 "capacitated" (Fig. 6*A*, Cap + H89) cells. In all cases, the amount of activity was normalized to the amount of EL present with an immunoblot, as per Fig. 3.

Sialylation of N612 Inhibits ACO2 Activity—Spermatozoa are catabolic in nature and, as such, it is not a surprise that the majority of Sia residues are lost during capacitation. However, in this study, we observed one enzyme that had an increase in sialylation, namely ACO2. To further understand this finding, we measured total Aconitase activity before and following mouse capacitation. As shown, during capacitation a statistically significant decrease in the level of Aconitase activity was observed (Fig. 7). Although this measurement would include both cytoplasmic and mitochondrial Aconitase activity, we reasoned that sperm have little cytoplasm, therefore, the bulk of Aconitase activity should be from the mitochondrial form.

To confirm that a decrease in ACO2 activity occurs specifically through sialylation at N612, we made both WT and Sia mimic, whereby the N612 was replaced by the negatively charged Aspartic acid (N612D). In both cases (WT and mimic), we made a GFP- and a HIS-tagged separate proteins.

Expression of the GFP-tagged proteins showed both WT and mutant proteins appeared be expressed in the mitochondiral (Fig. 8*A*). To confirm this, we co-localized GFP expression with the mitochondrial marker Mitotracker (Fig. 8*A*). Of interest, under fluorescence microscopy, we also noted a decrease in the level of GFP-tagged mutant, yet the number

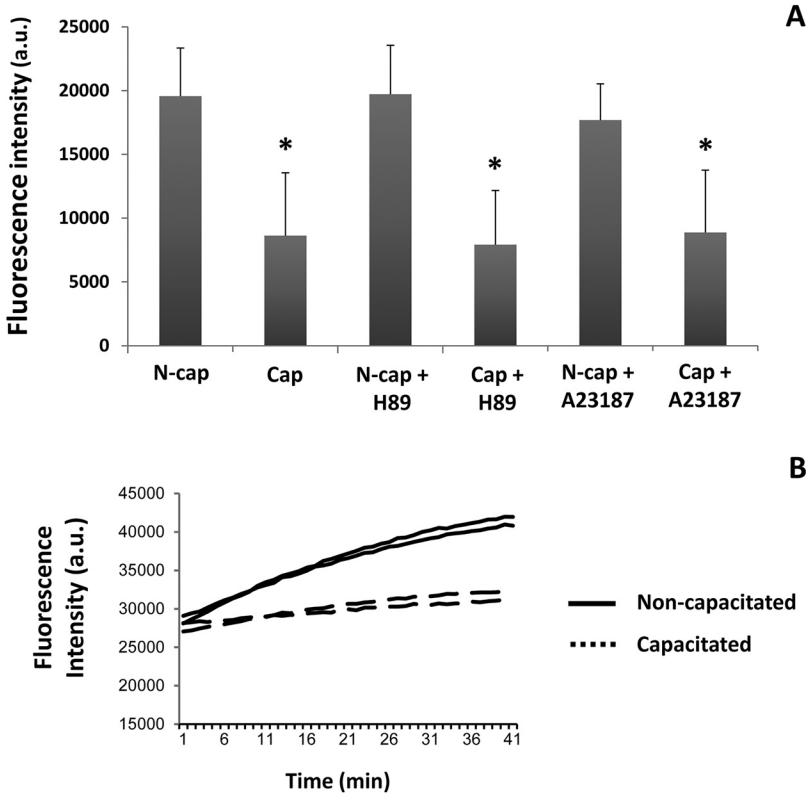

FIG. 6. Phospholipase A_1 (PLA_1) activity and the effect of the addition of A23187 and the PKA inhibitor H89 on non- and capacitated mouse spermatozoa. Enzyme activity was measured using the fluorescent PED-A_1 substrate. *A*, PLA_1 activity rate, within the first 10 min, for sperm cells previously incubated in noncapacitating or capacitating media with or without H89 and A23187. Image represents the mean value of five biological experiments. *B*, Example of the raw data for two noncapacitated (*solid line*) and two capacitated (dotted line) samples.

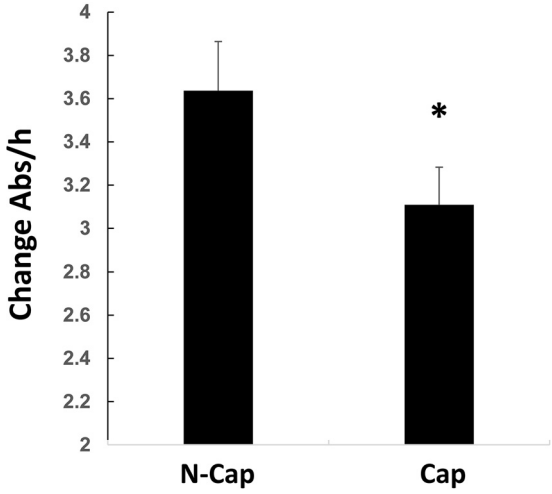

FIG. 7. Decrease in Aconitase activity during capacitation. Spermatozoa from mice were retrieved and incubated under non- or capacitating conditions. Following protein extraction, Aconitase activity was measured. To ensure equal amounts of Aconitase were present, the lysate was precipitated, run into SDS page, transferred and probed using anti-Aconitase antibody. The data shown is the average (± S.D.) of four biological replicates. Asterisk represents statistical significance ($p < 0.01$).

of cells transfected was equal (not shown). To determine if this was the case, we ran the cells through flow-cytometry. Analysis demonstrated that, in every replicate, the same number of cells were transfected (on average 35%), however, the mean level of GFP-fluorescence was significantly lower in the N612D-Aconitase expressing cells. For example, the histogram on Figs. 8*B* and 8*C* demonstrates that the peak height for GFP fluorescence in WT is slightly higher (Fig. 8*B*, black downward arrow) than in the N612D mutant (Fig. 8*C*, black downward arrow). This suggests that cells are less favorable to the expression of the N612D mutant over the WT. To confirm this hypothesis, we ran a SDS gel, transferred and probed it with antibodies against GFP- (Fig. 8*E*) or $(His)_6$-tagged proteins (not shown). When we probed equal number of transfected cells 24 or 48 h post transfection with anti-GFP (Fig. 8*E*), it was evident that less fusion protein was present in the N612D cells.

We next measured the ACO2 activity of the WT and N612D mutant (Fig. 9*A*). The use of equal amounts of recombinant protein was confirmed by immunoblotting. Remarkably, even when left overnight, we were unsuccessful in obtaining any ACO2 activity from the N612D mutant. In contrast, we could easily detect WT ACO2 activity. When put together, these datasets suggest that a switch in the ACO2 activity occurs during capacitation. This change in activity pattern is likely related to the modifications in the metabolic pathways described during the capacitation of mouse spermatozoa (*i.e.* from the oxidative phosphorylation pathway to the glycolytic pathway).

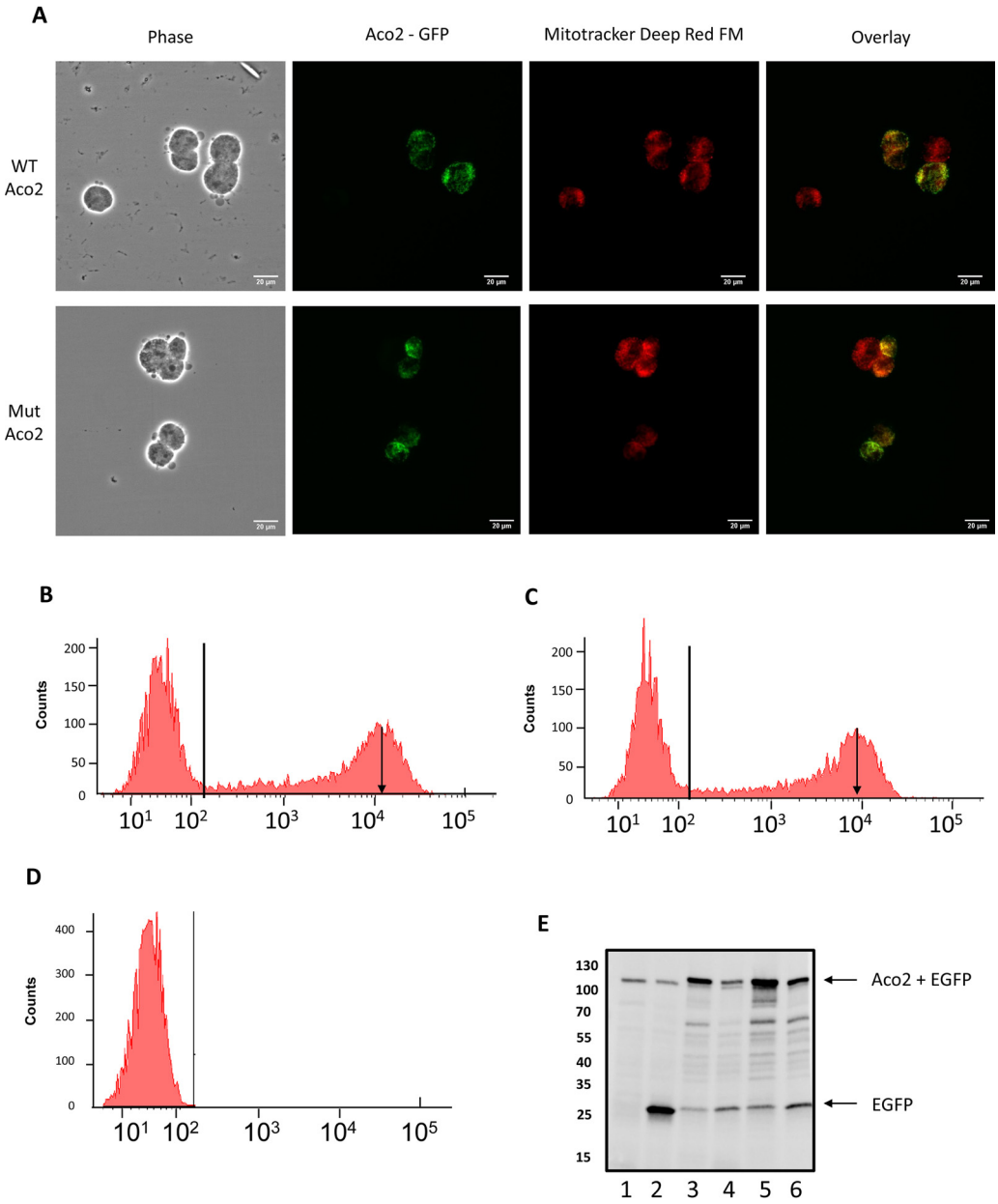

FIG. 8. Following cloning and insertion of the Aconitase gene into plasmid, site directed mutagenesis was used to create the N612D mutant. *A*, HEK293 cells were transiently transfected with GFP-tagged WT (top panels) or N612D mutant (bottom panels). Both proteins co-localized with the mitochondrial marker Mitotracker (Fig. 8*A*). Scale bar = 20 μM. *B–D*, Transfected cells were run through flow cytometer. Shown is the FL-1 channel *versus* counts of (*B*) GFP-tagged WT or (*C*) GFP-tagged N612D mutant. Arrow points to the mean signal intensity for each sample. Horizontal line represents the gate used for cell counting. *D*, shows signal from nontransfected cells. *E*, Relative amount of GFP-fusion protein for nontransfected cells (lane 1), GFP only vector (lane 2), WT (lanes 3and 5) or mutant (lanes 4 and 5) at either 24 h (lanes 2,3,4) or 48 h post-transfection (lanes 5–6).

Modeling the Bound Sialoglycoprotein to Aconitate Hydratase—To understand the impact sialylation would have on N612, we modeled its effect. Published crystal structures of Aconitate hydratase (46–49) and our highly homologous model, describes a large macromolecular structure comprising of four distinct domains employing a [4Fe-4S] cluster to catalyze the stereospecific dehydration of citrate to isocitrate (50). Within the enzyme itself, sits several highly conserved amino acids, such as Asp192, His194 and Arg607 that are crucial for ACO2 activity (shown in Fig. 9*B*). N612 resides on a short α-helical element immediately atop the active site, in an area often denoted as domain 4 [51]. To fit a Sia residue with N612, multiple changes in rotamers of sidechains were required. This allowed the formation of

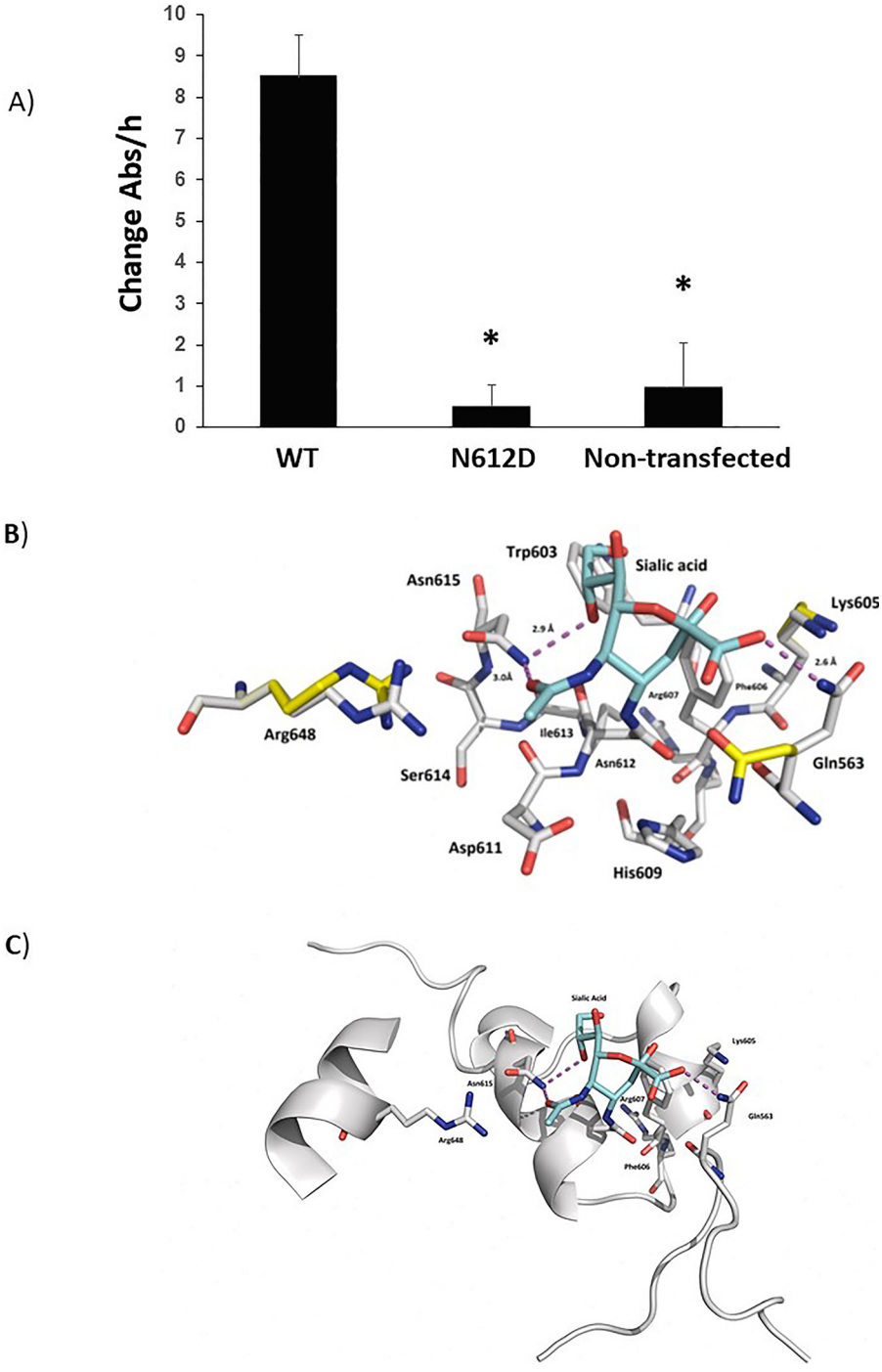

FIG. 9. *A*, N612D-mutant Aconitase displays no activity. HEK293 cells were transiently transfected with $(His)_6$-tagged WT and $(His)_6$-tagged N612D mutant. Aconitase was purified over nickel beads, run in SDS-PAGE and the immunoblotting performed to ensure that equal amounts of protein were used. Bars demonstrate the average ($n = 6$) activity of Aconitase with S.D. Nontransfected cells were used as controls. *B*, Ball and stick together with (*C*) ribbon model of aconitase. The different amino acids are labeled as shown. The purple dotted line represents hydrogen bonding. Shown is sialic acid (bluestructure) docked onto Asparagine 612 (Asn612).

new salt bridges and hydrogen bonds between the sugar and the α-helical structure, including the residue N614 (Asn615) and Gln563 that is present on an adjacent loop (Fig. 9 *B*, 9*C*). These data suggests that inhibition of ACO2 activity, through sialylation of Asparagine 612, is because of major distortion of the active site, which prevents catalysis from occurring.

DISCUSSION

Despite the importance of capacitation, the molecular mechanisms underlying this process are not yet fully understood. Previous studies have suggested that one facet of capacitation is a loss in Sia residues, which may be modulated by one (humans) or two (mouse) neuraminidases, namely neuraminidase 1 and 3 (28). In the present study,

using a LC–MS/MS-based approach, we were able to investigate capacitation-related changes of *N*-linked glycoproteins bearing terminal Sia. Surprisingly, we found little regulation of Sia within proteins groups following *in vitro* capacitation, with only 6.3% (9 of 142 peptides) demonstrating a significant change.

According to our data, the enzyme EL is one of the sperm proteins in which the Sia content is altered during capacitation. Previous studies have shown that four (N62, N118, N375, and N473) of the five potential N-glycosylation sites of human EL are occupied by glycan moieties (52, 53). In the present study, the sugar moiety at the N62 glycosylation site of EL was found to contain Sia in its structure. In addition, the peptide containing this glycosylation site was significantly reduced after *in vitro* capacitation, even though both quantity and molecular weight of EL remained unchanged. This suggests that a loss of a small glycan moiety or of a Sia residue itself occurs within EL during capacitation. Notably, a sialylated N-glycan structure at the corresponding glycosylation site (N64) has also been identified by our group in the EL of rat sperm (34). In this case, spermatozoa were taken from the caput, corpus and cauda regions of the epididymis. Remarkably, the Sia residue within EL was only found in spermatozoa derived from the caudal location. Furthermore, we have observed that the amount of EL within rat spermatozoa does not change, suggesting that Sia is added to EL during epididymal transit (data not published (34)). Given that Sia residues are removed from the same glycosylation site during capacitation, it is likely that this glycan moiety plays a specific role in regulating EL enzyme activity.

The glycosylation site at N62 of mouse EL is a conserved feature among animals and other members of the triglyceride lipase gene family, such as lipoprotein lipase and hepatic lipase. Using recombinant proteins, two separate studies have produced point mutations of the amino acids that are glycosylated in EL. Interestingly, in both cases, the loss of N62 led to increased EL activity (52, 53). Because of their negative charge and hydrophilicity, Sia residues within this glycan moiety could influence the structure and/or substrate specificity of EL, therefore, regulating its enzymatic activity. Of note however, we observed a decrease in the PLA_1 activity of EL following reduction of its sialylated glycopeptides (N62 glycosylation site) during capacitation. We can only assume that, besides the loss of N62, EL is likely to be regulated in other (yet unknown) ways to switch off its activity.

In addition to EL, we found that N612 sialylation of ACO2 increase following *in vitro* capacitation. This enzyme catalyzes the nonredox reaction of the TCA cycle in which stereospecific isomerization of citrate to isocitrate occurs (54). Adequate supply of ATP is essential to support capacitation-associated changes such as hyperactivation (55). In mouse, there is one report that suggests there is a switch from oxidative phosphorylation over to glycolysis (6). As such noncapacitated sperm demonstrated high oxygen consumption, which diminished as sperm capacitated, suggestion a mechanism to switch over to glycolysis (6). One potential switch could be brought about through sialylation of ACO2, particularly N612. Indeed, modeling of the enzyme suggests that this Asparagine residue sits atop of the ACO2 activity site (Fig. 9) in a highly conserved region. Analyses of multiple x-ray crystal structures of Aconitate hydratase has shown that a vast array of residues from all four domains of the enzyme are required to carry out catalysis (56), whether it is to bind and recognize substrate or ligate the [4Fe-4S] cluster. Similarly, this complex array, dependent on bound ligands, displays several nuanced and obvious conformational changes within its active site and other domains (56). Thus, it is apparent that in our model, inhibition likely occurs through segmental conformational change of the antiparallel helical motif that N612 is a part (residues 606-612 in our model; Fig. 9). Considering this includes the active site residue Arg607, it is possible that changes in substrate binding may occur to prevent catalysis, such as a rotameric shifts or larger domain movements that may prevent substrate binding and release, a trait often linked with *N*-linked glycosylation (57). A caveat to this study is despite making the N612D, mutant, modeling demonstrates we can only compare this to the WT and not a second (for example) neutral amino acid mutant substitution. The latter would appear to cause major hydrogen bonding and solvent exposure changing to at least 5 different amino acids, the result being total loss of enzyme activity. However, the loss of activity was not because of the negative charge a sialic acid residue would confer, but rather because of complete confirmation change of the active site. As such, without the neutral substitution, our data really demonstrate that the active site is very susceptible to any change.

Inspection of Uniprot suggests that the glycosylation at N612 has never been reported in any other cell type and, as such, may represent a novel mechanism, attributed just to sperm cells. Unfortunately, compounds to block or inhibit sialic acid transferases are not cell permeable and, for this reason, we were unable to directly ascribe the significance of a lack of ACO2 activity to sperm physiology. Additionally, an indiscriminate blockage of sialyltransferases would have raised doubts about what other proteins/pathways could also have been co-inhibited and this obfuscated the interpretation. Our leading hypothesis is that glycolysis is required for the rapid movement of the sperm flagella, in a process known as hyperactivation. The latter being essential for fertilization to occur. Therefore, sperm cells being transcriptionally and translationally silent cells may change ACO2 activity via sialylation of this protein, which facilitates the shuttling of its metabolic process from oxidative phosphorylation over to glycolysis.

DATA AVAILABILITY

The raw files used for this project can be accessed from the MassIVE database (MassIVE ID: MSV000085806, doi: https://doi.org/10.25345/C5VX6V).

Funding and additional information—This work was supported by the Brazilian National Council for Scientific and Technological Development (CNPq).

Author contributions—A.I.S.B.V., J.K.N., and M.A.B. designed research; A.I.S.B.V. and R.A.O. performed research; A.I.S.B.V., R.A.O., V.C., J.K.N., and M.A.B. analyzed data; A.I.S.B.V., P.L., V.C., T.V., J.K.N., and M.A.B. wrote the paper; P.L., J.K.N., and M.A.B. contributed new reagents/analytic tools.

Conflict of interest—The authors declare that they have no conflicts of interest with the contents of this article.

Abbreviations—The abbreviations used are: ACN, acetonitrile; Arg, Arginine; N or Asn, Asparagine; dbcAMP, dibutyryl-cAMP; EL, endothelial lipase; Gln, Glutamic acid; His, Histidine; LC-MS/MS, liquid chromatography tandem-mass spectrometry; Lys, Lysine; MS, mass spectrometry; MAM, meprin/A5 antigen/mu receptor tyrosine phosphatase; ACO_2, mitochondrial aconitate hydratase; PNGase F, peptide-N-glycosidase F; PLA_1, phospholipase A1; PED-A_1, phospholipase A1 selective substrate; Ser, Serine; Sia, sialic acid; Thr, Threonine; D or Asp, Aspartic acid; TiO_2, titanium dioxide; TCA, tricarboxylic acid; TFA, trifluoroacetic acid; ACO_2, aconitate hydratase ; WT, wild-type transfected.

Received April 28, 2020, and in revised form, July 22, 2020 Published, MCP Papers in Press, August 24, 2020, DOI 10.1074/mcp.RA120.002109

REFERENCES

1. Chang, M. C. (1951) Fertilizing capacity of spermatozoa deposited into the fallopian tubes. *Nature* **168,** 697–698
2. Austin, C. (1952) The 'capacitation'of the mammalian sperm. *Nature* **170,** 326–326
3. Visconti, P. E., Bailey, J. L., Moore, G. D., Pan, D., Olds-Clarke, P., and Kopf, G. S. (1995) Capacitation of mouse spermatozoa. I. Correlation between the capacitation state and protein tyrosine phosphorylation. *Development* **121,** 1129–1137
4. Visconti, P. E., Moore, G. D., Bailey, J. L., Leclerc, P., Connors, S. A., Pan, D., Olds-Clarke, P., and Kopf, G. S. (1995) Capacitation of mouse spermatozoa. II. Protein tyrosine phosphorylation and capacitation are regulated by a cAMP-dependent pathway. *Development* **121,** 1139–1150
5. Baker, M. A. (2016) Proteomics of post-translational modifications of mammalian spermatozoa. *Cell Tissue Res*. **363,** 279–287
6. Fraser, L. R., and Lane, M. (1987) Capacitation-and fertilization-related alterations in mouse sperm oxygen consumption. *J. Reprod. Fertil*. **81,** 385–393
7. Miki, K., Qu, W., Goulding, E. H., Willis, W. D., Bunch, D. O., Strader, L. F., Perreault, S. D., Eddy, E. M., and O'Brien, D. A. (2004) Glyceraldehyde 3-phosphate dehydrogenase-S, a sperm-specific glycolytic enzyme, is required for sperm motility and male fertility. *Proc. Natl. Acad. Sci. U S A* **101,** 16501–16506
8. Baker, M. A. (2011) The'omics revolution and our understanding of sperm cell biology. *Asian J. Androl*. **13,** 6–10
9. Baker, M. A., Nixon, B., Naumovski, N., and Aitken, R. J. (2012) Proteomic insights into the maturation and capacitation of mammalian spermatozoa. *Syst. Biol. Reprod. Med*. **58,** 211–217
10. Ficarro, S., Chertihin, O., Westbrook, V. A., White, F., Jayes, F., Kalab, P., Marto, J. A., Shabanowitz, J., Herr, J. C., Hunt, D. F., and Visconti, P. E. (2003) Phosphoproteome analysis of capacitated human sperm evidence of tyrosine phosphorylation of a kinase-anchoring protein 3 and valosin-containing protein/p97 during capacitation. *J. Biol. Chem*. **278,** 11579–11589
11. Porambo, J. R., Salicioni, A. M., Visconti, P. E., and Platt, M. D. (2012) Sperm phosphoproteomics: historical perspectives and current methodologies. *Expert Rev. Proteomics*. **9,** 533–548
12. Brewis, I. A., and Gadella, B. M. (2010) Sperm surface proteomics: from protein lists to biological function. *Mol. Hum. Reprod*. **16,** 68–79
13. Varki, A. (1993) Biological roles of oligosaccharides: all of the theories are correct. *Glycobiology* **3,** 97–130
14. Lowe, J. B., and Marth, J. D. (2003) A genetic approach to mammalian glycan function. *Annu. Rev. Biochem*. **72,** 643–691
15. Fei, W., and Hao, X. (1990) Wheat germ agglutinin (WGA) receptors on human sperm membrane and male infertility. *Arch. Androl*. **24,** 97–97
16. Jiménez, I., Gonzalez-Marquez, H., Ortiz, R., Betancourt, M., Herrera, J., and Fierro, R. (2002) Expression of lectin receptors on the membrane surface of sperm of fertile and subfertile boars by flow cytometry. *Arch. Androl*. **48,** 159–166
17. Steele, M., and Wishart, G. (1996) Demonstration that the removal of sialic acid from the surface of chicken spermatozoa impedes their transvaginal migration. *Theriogenology* **46,** 1037–1044
18. Yudin, A. I., Generao, S. E., Tollner, T. L., Treece, C. A., Overstreet, J. W., and Cherr, G. N. (2005) Beta-defensin 126 on the cell surface protects sperm from immunorecognition and binding of anti-sperm antibodies. *Biol. Reprod*. **73,** 1243–1252
19. Ma, X., Pan, Q., Feng, Y., Choudhury, B. P., Ma, Q., Gagneux, P., and Ma, F. (2016) Sialylation facilitates the maturation of mammalian sperm and affects its survival in female uterus. *Biol. Reprod*. **94,** 123 121–110
20. Tollner, T. L., Yudin, A. I., Treece, C. A., Overstreet, J. W., and Cherr, G. N. (2008) Macaque sperm coating protein DEFB126 facilitates sperm penetration of cervical mucus. *Hum. Reprod*. **23,** 2523–2534
21. Focarelli, R., Giuffrida, A., and Rosati, F. (1995) Changes in the sialylglycoconjugate distribution on the human sperm surface during in-vitro capacitation: partial purification of a 20 kDa sialylglycoprotein of capacitated spermatozoa. *Mol. Hum. Reprod*. **1,** 369–373
22. Mahmoud, A., and Parrish, J. (1996) Oviduct fluid and heparin induce similar surface changes in bovine sperm during capacitation: a flow cytometric study using lectins. *Mol. Reprod. Dev*. **43,** 554–560
23. Medeiros, C., and Parrish, J. (1996) Changes in lectin binding to bovine sperm during heparin-induced capacitation. *Mol. Reprod. Dev*. **44,** 525–532
24. Jiménez, I., González-Márquez, H., Ortiz, R., Herrera, J. A., García, A., Betancourt, M., and Fierro, R. (2003) Changes in the distribution of lectin receptors during capacitation and acrosome reaction in boar spermatozoa. *Theriogenology* **59,** 1171–1180
25. Rosado, A., Velázquez, A., and Lara-Ricalde, R. (1973) Cell polarography. II. Effect of neuraminidase and follicular fluid upon the surface characteristics of human spermatozoa. *Fertil. Steril*. **24,** 349–354
26. Iqbal, N., and Hunter, A. (1995) Comparison of various bovine sperm capacitation systems for their ability to alter the net negative surface charge of spermatozoa. *J. Dairy Sci*. **78,** 84–90
27. Focarelli, R., Rosati, F., and Terrana, B. (1990) Sialylglycoconjugates release during in vitro capacitation of human spermatozoa. *Journal of andrology* **11,** 97–104
28. Ma, F., Wu, D., Deng, L., Secrest, P., Zhao, J., Varki, N., Lindheim, S., and Gagneux, P. (2012) Sialidases on mammalian sperm mediate deciduous sialylation during capacitation. *J. Biol. Chem*. **287,** 38073–38079
29. Davis, B. K., Byrne, R., and Bedigian, K. (1980) Studies on the mechanism of capacitation: albumin-mediated changes in plasma membrane lipids during in vitro incubation of rat sperm cells. *Proc. Natl. Acad. Sci. U S A* **77,** 1546–1550
30. Baker, M. A., Krutskikh, A., Curry, B. J., McLaughlin, E. A., and Aitken, R. J. (2004) Identification of cytochrome P450-reductase as the enzyme

responsible for NADPH-dependent lucigenin and tetrazolium salt reduction in rat epididymal sperm preparations. *Biol. Reprod*. **71,** 307–318
31. Baker, M. A., Krutskikh, A., Curry, B. J., Hetherington, L., and Aitken, R. J. (2005) Identification of cytochrome-b5 reductase as the enzyme responsible for NADH-dependent lucigenin chemiluminescence in human spermatozoa. *Biol. Reprod*. **73,** 334–342
32. Daniel, J. C. Jr (1971) Methods in mammalian embryology. In *Methods in mammalian embryology*, ed. Freeman, pp. 532, San Francisco
33. Wessel, D., and Flugge, U. I. (1984) A method for the quantitative recovery of protein in dilute solution in the presence of detergents and lipids. *Anal. Biochem*. **138,** 141–143
34. Villaverde, A. I. S. B., Hetherington, L., and Baker, M. A. (2016) Quantitative glycopeptide changes in rat sperm during epididymal transit. *Biol. Reprod*. **94,** 91, 1–13
35. Baker, M. A., Naumovski, N., Hetherington, L., Weinberg, A., Velkov, T., and Aitken, R. J. (2013) Head and flagella subcompartmental proteomic analysis of human spermatozoa. *Proteomics* **13,** 61–74
36. Darrow, A. L., Olson, M. W., Xin, H., Burke, S. L., Smith, C., Schalk-Hihi, C., Williams, R., Bayoumy, S. S., Deckman, I. C., Todd, M. J., Damiano, B. P., and Connelly, M. A. (2011) A novel fluorogenic substrate for the measurement of endothelial lipase activity. *J. Lipid Res*. **52,** 374–382
37. McCoy, M. G., Sun, G.-S., Marchadier, D., Maugeais, C., Glick, J. M., and Rader, D. J. (2002) Characterization of the lipolytic activity of endothelial lipase. *J. Lipid Res*. **43,** 921–929
38. Seu, K. J., Cambrea, L. R., Everly, R. M., and Hovis, J. S. (2006) Influence of lipid chemistry on membrane fluidity: tail and headgroup interactions. *Biophys. J*. **91,** 3727–3735
39. Dawaliby, R., Trubbia, C., Delporte, C., Noyon, C., Ruysschaert, J.-M., Van Antwerpen, P., and Govaerts, C. (2016) Phosphatidylethanolamine is a key regulator of membrane fluidity in eukaryotic cells. *J. Biol. Chem*. **291,** 3658–3667
40. McCallum, C. D., and Epand, R. M. (1995) Insulin receptor autophosphorylation and signaling is altered by modulation of membrane physical properties. *Biochemistry* **34,** 1815–1824
41. Inoue, N., Hirata, K., Yamada, M., Hamamori, Y., Matsuda, Y., Akita, H., and Yokoyama, M. (1992) Lysophosphatidylcholine inhibits bradykinin-induced phosphoinositide hydrolysis and calcium transients in cultured bovine aortic endothelial cells. *Circ. Res*. **71,** 1410–1421
42. Lundbaek, J. A., and Andersen, O. S. (1994) Lysophospholipids modulate channel function by altering the mechanical properties of lipid bilayers. *J. Gen. Physiol*. **104,** 645–673
43. Owens, K., Kennett, F. F., and Weglicki, W. B. (1982) Effects of fatty acid intermediates on Na+-K+-ATPase activity of cardiac sarcolemma. *Am. J. Physiol*. **242,** H456–H461
44. Salicioni, A. M., Platt, M. D., Wertheimer, E. V., Arcelay, E., Allaire, A., Sosnik, J., and Visconti, P. E. (2007) Signalling pathways involved in sperm capacitation. *Soc. Reprod. Fertil. Suppl*. **65,** 245–259
45. Roldan, E., and Shi, Q. (2007) Sperm phospholipases and acrosomal exocytosis. *Front. Biosci*. **12,** 89–104
46. Lloyd, S., Lauble, H., Prasad, G., and Stout, C. (1999) The mechanism of aconitase: 1.8 Å resolution crystal structure of the S642A: citrate complex. *Protein Sci*. **8,** 2655–2662
47. Lauble, H., Kennedy, M., Emptage, M., Beinert, H., and Stout, C. (1996) The reaction of fluorocitrate with aconitase and the crystal structure of the enzyme-inhibitor complex. *Proceedings of the National Academy of Sciences* **93,** 13699–13703
48. Lauble, H., Kennedy, M. C., Beinert, H., and Stout, C. D. (1994) Crystal structures of aconitase with trans-aconitate and nitrocitrate bound. *J. Mol. Biol*. **237,** 437–451
49. Robbins, A., and Stout, C. (1989) Structure of activated aconitase: formation of the [4Fe-4S] cluster in the crystal. *Proc. Natl. Acad. Sci. U S A* **86,** 3639–3643
50. Beinert, H., Kennedy, M. C., and Stout, C. D. (1996) Aconitase as iron−sulfur protein, enzyme, and iron-regulatory protein. *Chem. Rev*. **96,** 2335–2374
51. Dupuy, J., Volbeda, A., Carpentier, P., Darnault, C., Moulis, J.-M., and Fontecilla-Camps, J. C. (2006) Crystal structure of human iron regulatory protein 1 as cytosolic aconitase. *Structure* **14,** 129–139
52. Miller, G. C., Long, C. J., Bojilova, E. D., Marchadier, D., Badellino, K. O., Blanchard, N., Fuki, I. V., Glick, J. M., and Rader, D. J. (2004) Role of N-linked glycosylation in the secretion and activity of endothelial lipase. *J. Lipid Res*. **45,** 2080–2087
53. Skropeta, D., Settasatian, C., McMahon, M. R., Shearston, K., Caiazza, D., McGrath, K. C., Jin, W., Rader, D. J., Barter, P. J., and Rye, K.-A. (2007) Rye K-A: N-Glycosylation regulates endothelial lipase-mediated phospholipid hydrolysis in apoE-and apoA-I-containing high density lipoproteins. *J. Lipid Res*. **48,** 2047–2057
54. Beinert, H., and Kennedy, M. C. (1993) Aconitase, a two-faced protein: enzyme and iron regulatory factor. *FASEB J*. **7,** 1442–1449
55. Ferramosca, A., and Zara, V. (2014) Bioenergetics of mammalian sperm capacitation. *BioMed Res. Int*. **2014,** 902953
56. Lauble, H., and Stout, C. D. (1995) Steric and conformational features of the aconitase mechanism. *Proteins: Structure, Function, and Bioinformatics* **22,** 1–11
57. Imperiali, B., and O'Connor, S. E. (1999) Effect of N-linked glycosylation on glycopeptide and glycoprotein structure. *Curr. Opin. Chem. Biol*. **3,** 643–649